

# Simplified modeling of cluster-shell competition in $^{20}\text{Ne}$ and $^{24}\text{Mg}$

N. Itagaki<sup>1</sup>, J. Cseh<sup>2</sup>, and M. Płoszajczak<sup>3</sup>

<sup>1</sup>*Yukawa Institute for Theoretical Physics, Kyoto University,  
Kitashirakawa Oiwake-Cho, 606-8502 Kyoto, Japan*

<sup>2</sup>*Institute of Nuclear Research of the Hungarian Academy of Sciences, Debrecen, Pf. 51, Hungary-4001*

<sup>3</sup>*Grand Accélérateur National d'Ions Lourds (GANIL),  
CEA/DSM – CNRS/IN2P3, BP 5027, F-14076 Caen Cedex 05, France*

(Dated: December 20, 2010)

We investigate properties of the Generator Coordinate Method (GCM) on a collective basis of Antisymmetrized Quasi-Cluster (AQC) states to describe the cluster-shell competition in  $^{20}\text{Ne}$  and  $^{24}\text{Mg}$  due to the spin-orbit interaction. By introducing a single additional parameter in the antisymmetrized-cluster basis function, a continuous transformation of the  $\alpha$  cluster(s) into independent nucleons can be described. We apply this GCM trial wave function to study in details the transition from cluster states [ $^{16}\text{O}+\alpha$ ] and [ $^{16}\text{O}+\alpha+\alpha$ ] to shell model (SM) states [ $^{16}\text{O}+4\text{N}$ ] and [ $^{16}\text{O}+8\text{N}$ ], respectively. An optimal value of the strength of the spin-orbit interaction is deduced by reproducing level spacing in  $^{20}\text{Ne}$ . A possible connection to the group theoretical understanding of the cluster-shell configuration transition is also discussed.

PACS numbers: 21.30.Fe, 21.60.Cs, 27.20.+n, 27.30.+t, 21.60Fw, 21.60Gx

## I. INTRODUCTION

Atomic nuclei provide a rich diversity of properties typical for mesoscopic systems. One of standard features of these systems is the mean field and the associated shell structure. Indeed, the single-particle motion is a cornerstone of nuclear structure [1] and the stability of nuclei depends on non-uniformities of the single-particle level distribution and presence of magic gaps. Contrary to atomic systems, a strong spin-orbit interaction is a key ingredient to fully explain the observed magic numbers in atomic nuclei [2, 3]. Another important aspect of nuclear structure is the clustering phenomenon which is of particular importance in states close to their cluster decay thresholds [4] due to generic features of the continuum coupling [5, 6]. In this context  $\alpha$ -particle, which is strongly bound and  $\alpha$ - $\alpha$  interaction is not strong enough to make a bound state, can be considered as an effective building block of the nuclear structure. Indeed, many features of nuclear masses and excitations in even-even  $N = Z$  light nuclei can be explained by (2n-2p) quarteting effects [7]. This molecular viewpoint has been introduced by Wheeler, von Weizsäcker and Wefelmeier [8] long before the nuclear Shell Model (SM) has been proposed [2, 3], and cluster structures have been extensively studied for more than four decades [9–15] (for a selection of recent works, see Ref. [16]). Recently, theoretical and experimental investigations of clustering phenomena have been extended towards neutron-rich nuclei [17, 18] (see Ref. [19] for a recent review).

If an  $\alpha$ -cluster is expressed as the lowest  $(s_{1/2})^4$  SM configuration, it is a spin-zero system where only the central interactions contributes. The stability of such a cluster and, hence, its physical significance is closely related to the respective role of different components of the nuclear interaction in building shell structure and nuclear excitations. Hence, the cluster-shell competition is

a key issue to understand how effective building blocks of nuclear structure arise from complex nuclear forces. Usually, this competition is studied at the level of two-nucleon forces only but it is expected that three-nucleon forces and four-nucleon forces may play some role in this problem as well. Another important issue in this discussion is the role of coupling to the decay channels which would require the open quantum system formulation of the many-body problem, as provided by the Continuum Shell Model (for recent reviews see Refs. [5, 20, 21]). These two important issues will not be considered in this paper.

Being interested in the shell or cluster nature of a nuclear state the shell and cluster models, and their interrelation can guide us. In general both of these models provide us with a complete (or overcomplete) set of basis states, until we speak about the general shell and cluster models, without severe truncations which are necessarily applied in practical applications (see e.g. the specific models applied later on in this article). It means that any state can be expanded in both basis. Then there are four different possibilities. (i) The expansion in the shell model basis is simple, but in the cluster basis is complicated; we can call these states as shell-model-like (SM) states. (ii) The expansion in the cluster model basis is simple, but in the shell basis is complicated; we can call these states as cluster-model-like (CM) states (sometimes they are called rigid molecule-like cluster states). (iii) The expansion is simple both in the shell model basis and in the cluster basis; we can call these states as shell-model-like cluster (SMC) states. (iv) The expansion is complicated both in the shell model basis and in the cluster basis; these states are not interesting from our present viewpoint. (For a recent discussion, see Ref. [22] and references cited therein). In favorable cases, states (i)-(iii) can be characterized by simple symmetries. For example, SM states in the superconducting limit obey  $\text{SU}(2)$  sym-

metry, rigid molecule-like cluster states can have  $SO(4)$  symmetry, while states with  $SU(3)$  symmetry have good shell and cluster nature at the same time.

In this work, we aim at obtaining a transparent picture of the cluster-shell competition based on studies of both binding energies and complex spectra. Hence, even though different microscopic studies of the cluster-shell competition are currently possible [23, 24], we apply here the GCM [25] on a simple, flexible basis of Antisymmetrized Quasi-Cluster (AQC) states [26, 27], where the cluster-shell transition is described by a single parameter. The AQC parameterization is used here to extract the information about the cluster-shell competition in  $^{20}\text{Ne}$  and  $^{24}\text{Mg}$  in various spatial configurations and for different values of the strength of the spin-orbit interaction.

Recently, a considerable interest is devoted to studying quantum phases and phase-transitions in algebraic models. (For a recent review, see [28, 29] and references cited therein.). The transition from a cluster state to the SM state when changing a control-parameter, seems to be analogous to this problematic. Therefore, we discuss in this paper similarities and differences between the present GCM+AQC approach and the algebraic approach. As a result of this comparison, a possible algebraic calculation is outlined for a further study of the cluster-shell competition.

This paper is organized as follows. The formulation of the model and details of the AQC approach are summarized in section II. In section III, we present results concerning the cluster-shell competition in  $^{20}\text{Ne}$  and  $^{24}\text{Mg}$ . In particular, we exhibit the evolution of wave functions for different low spin states of  $^{20}\text{Ne}$  with the strength of the spin-orbit coupling by plotting the squared overlap between the variational GCM wave function and the AQC basis states. Possible connections to a group theoretical understanding of the cluster-shell transition is discussed in section IV. Finally, the main conclusions of this work are given in section V.

## II. THE MODEL

In this section, we introduce the GCM+AQC approach and the many-body Hamiltonian used in the cluster-shell transition studies of this work. Let us begin by presenting the basic idea of the AQC wave function and its relation to other parameterized cluster-like wave functions.

### A. The Brink-Bloch wave function

In conventional  $\alpha$ -cluster models, the single particle wave function is described as a Gaussian packet [11]:

$$\psi_i = \left(\frac{2\nu}{\pi}\right)^{\frac{3}{4}} \exp[-\nu(\vec{r}_i - \vec{R}_\gamma/\sqrt{\nu})^2] \chi_i, \quad (1)$$

where  $\chi_i$  represent the spin-isospin part of the  $i$ -th single particle, and  $R_\gamma$  is a real parameter representing the center of a Gaussian for  $\gamma$ -th  $\alpha$ -cluster. To assure that the spurious center-of-mass kinetic energy is exactly removed, the parameter  $\nu$  is the same for *all* nucleons. In this Brink-Bloch wave function [11], four nucleons (spin-up proton/neutron, spin-down proton/neutron) share the common  $R_\gamma$  value. Hence, the spin-orbit interaction vanishes for Brink-Bloch  $\alpha$ -clusters. In general, even if there are valence nucleons around clusters, the spin-orbit interaction vanishes for a single Slater determinant wave function because the time-odd components in the spatial part of such a wave function are missing [30]. Hence, the contribution of the spin-orbit interaction for valence nucleons around  $\alpha$ -cluster(s) can be taken into account only by performing the angular momentum projection and/or by superposing the Slater determinants with complex coefficients. However, for  $(N\alpha)$ -nuclei, the spin-orbit interaction does not act even after these treatments, since all clusters have spin zero.

### B. The AMD and FMD wave functions

In AMD [31] and Fermionic Molecular Dynamics (FMD) [32] approaches, both deriving from the Time-Dependent Cluster (TDC) approach [33], the Gaussian center parameters are allowed to be complex. In this case, the single particle wave functions contain time-odd components, and the spin-orbit interaction acts even at the level of a single Slater determinant, i.e. before the angular momentum projection. The single particle wave function of  $i$ -th nucleon has the following form:

$$\psi_i = \left(\frac{2\nu}{\pi}\right)^{\frac{3}{4}} \exp[-\nu(\vec{r}_i - \vec{z}_i/\sqrt{\nu})^2] \chi_i, \quad (2)$$

where  $\vec{z}_i$  is a complex parameter [34]. The real and imaginary parts of  $\vec{z}_i$  represent the expectation values of the position:  $\langle \vec{r} \rangle = \text{Re}[\vec{z}_i]/\sqrt{\nu}$ , and momentum:  $\langle \vec{p} \rangle = 2\sqrt{\nu}\hbar \text{Im}[\vec{z}_i]$ , of the  $i$ -th nucleon. Since this single particle wave function breaks the time-reversal symmetry, it allows to describe the boost of nuclei. Thus, this variational ansatz (2) for the wave function can be applied not only in static, nuclear structure calculations but also in dynamical nuclear reaction calculations [13, 14, 31, 35]. In the latter case, equations of motion for the time-evolution of parameters  $\{\vec{z}_i\}$  [33] are derived from the variational principle associated with the time-dependent Schrödinger equation [36].

### C. The AQC wave function

The AQC approach [26, 27] allows for a convenient transformation of the SM wave function in  $jj$  coupling scheme into the  $\alpha$ -cluster wave function. Hence, this approach is particularly well suited for studies of the

cluster-shell competition and a description of the mixed phase in terms of quasi-clusters, i.e. the SM-like cluster states. Let us suppose that the nucleus consists of few  $\alpha$ -clusters and one quasi-cluster. In general, one can also consider valence nucleons but to keep the discussion of the cluster-shell competition as transparent as possible, we shall restrict ourselves to systems consisting of  $\alpha$ -clusters and quasi-cluster(s). The Gaussian-center parameters  $\vec{z}_i/\sqrt{\nu}$  for nucleons in  $\alpha$ -clusters are real numbers. For nucleons in the quasi-cluster, the single-particle wave function is described as a Gaussian packet:

$$\psi_i = \left(\frac{2\nu}{\pi}\right)^{\frac{3}{4}} \exp[-\nu(\vec{r} - \vec{\zeta}_i/\sqrt{\nu})^2] \chi_i, \quad (3)$$

where  $\vec{\zeta}_i/\sqrt{\nu}$  are the generalized center parameters of the packet, and:

$$\vec{\zeta}_i = \vec{z}_i + i\Lambda(\vec{e}_{spin}^i) \times \text{Re}[\vec{z}_i]. \quad (4)$$

In the above equation,  $\vec{e}_{spin}^i$  is the unit vector for the intrinsic-spin orientation, and  $\Lambda$  is a control parameter describing the dissolution of the (quasi)-cluster.

The spin-orbit interaction is intuitively interpreted as  $(\vec{r} \times \vec{p}) \cdot \vec{s}$  and this is equal to  $(\vec{s} \times \vec{r}) \cdot \vec{p}$ , where  $\vec{r}$ ,  $\vec{p}$ , and  $\vec{s}$  represent the position, the momentum, and the spin of the nucleon, respectively. If nucleons of the quasi-cluster have the momentum components parallel (anti-parallel) to  $\vec{s} \times \vec{r}$ , the spin-orbit interaction acts attractively (repulsively), i.e. the spin-orbit coupling acts on each individual wave function. For positive (negative)  $\Lambda$ , the contribution of spin-orbit interaction is attractive (repulsive). In actual calculation, of course, the spin-orbit coupling is a two-body force, so this interaction is a function of  $\vec{r}_i - \vec{r}_j$  and not of  $\vec{r}$ .

Parameters  $\{\vec{z}_i\}$  and/or  $\Lambda$  are complex in the time-dependent formulation of nuclear reactions and dynamics. In the present studies, however, we perform static calculations, so  $\{\vec{z}_i\}$  and  $\Lambda$  are real. Hence, real and imaginary parts of the Gaussian-center parameters for nucleons of the quasi cluster are:

$$\begin{aligned} \text{Re}[\vec{\zeta}_i] &= \vec{z}_i \\ \text{Im}[\vec{\zeta}_i] &= \Lambda(\vec{e}_{spin}^i) \times \vec{z}_i. \end{aligned}$$

The real parts of  $\{\vec{\zeta}_i\}$ , are the same for four nucleons of the quasi cluster.

In the following sections, this parameterized wave function will be applied to explain observed levels in  $^{20}\text{Ne}$  and an evolution of the wave function with the strength of the spin-orbit coupling in  $^{20}\text{Ne}$  and  $^{24}\text{Mg}$ . In particular, it will be shown that the limits  $\Lambda = 0$  and  $\Lambda = 1$  of the AQC wave function correspond to the cluster wave function and the SM wave function (the spherical harmonics), respectively.  $\Lambda < 0$  describes a particle in spin-orbit unfavored orbits, whereas  $\Lambda > 1$  corresponds to a particle in higher shells.

## D. The Hamiltonian

The Hamiltonian operator ( $\hat{H}$ ) has the following form:

$$\hat{H} = \sum_{i=1}^A \hat{t}_i - \hat{T}_{c.m.} + \sum_{i>j}^A \hat{v}_{ij}, \quad (5)$$

where a two-body interaction ( $\hat{v}_{ij}$ ) includes the central part, the spin-orbit part and the Coulomb part. For the central part, we use the Volkov2 effective  $N-N$  potential [37]:

$$V(r) = (W - MP^\sigma P^\tau) \times [V_1 \exp(-r^2/c_1^2) + V_2 \exp(-r^2/c_2^2)], \quad (6)$$

where  $W = 1 - M$ ,  $V_1^c = -60.65$  MeV,  $V_2^c = 61.14$  MeV,  $c_1 = 1.8$  fm, and  $c_2 = 1.01$  fm. For the spin-orbit term, we introduce the two-range variant of the G3RS potential [38]:

$$V_{ls} = V_0(e^{-d_1 r^2} - e^{-d_2 r^2})P(^3\text{O})\vec{L} \cdot \vec{S}, \quad (7)$$

where  $d_1 = 5.0$  fm $^{-2}$ ,  $d_2 = 2.778$  fm $^{-2}$ , and  $P(^3\text{O})$  is a projection operator onto a triplet-odd state. The operator  $\vec{L}$  stands for the relative angular momentum and  $\vec{S} \equiv \vec{S}_1 + \vec{S}_2$  is the spin operator.

The parameter set:  $M = 0.60$  and  $V_0 = 2000$  MeV, is known to give a reasonable description of  $\alpha + n$  and  $\alpha + \alpha$  scattering phase shifts [39]. For heavier nuclei, beyond  $^{12}\text{C}$ , one needs however larger  $M$  values in the structure calculations. In the present study of energy levels in  $^{20}\text{Ne}$  and  $^{24}\text{Mg}$ , we take  $M = 0.62$  and compare experimental and calculated spectra for three values of the strength parameter  $V_0 = 0, 1000, 2000$  MeV.

## E. The GCM trial wave function

The trial wave function of an A-particle system is constructed in the form:

$$\Phi(\vec{r}_1, \dots, \vec{r}_A) = \int \Psi(\vec{r}_1, \dots, \vec{r}_A; \Lambda, R) f(\Lambda, R) d\Lambda dR \quad (8)$$

where  $f(\Lambda, R)$  is a variational function of GCM and  $\Psi(\vec{r}_1, \dots, \vec{r}_A; \Lambda, R)$  is a basis function:

$$\begin{aligned} \Psi(\vec{r}_1, \dots, \vec{r}_A; \Lambda, R) &= \\ \hat{P}^\pi \hat{P}_{MK}^J \mathcal{A}[(\psi_1(\vec{r}_1)\chi_1) \cdots (\psi_k(\vec{r}_k)\chi_k) \\ &\quad (\psi_{k+1}(\vec{r}_{k+1}; \Lambda, R)\chi_{k+1}) \cdots (\psi_A(\vec{r}_A; \Lambda, R)\chi_A)] \end{aligned} \quad (9)$$

$\hat{P}^\pi$  and  $\hat{P}_{MK}^J$  in (8) are projection operators on a good parity and angular momentum, respectively, and  $\psi_i$  and  $\chi_i$  represent the spatial and spin-isospin parts of the  $i$ -th single particle AQC wave function, respectively. The single particles from 1 to  $k$  belong to normal cluster(s)

and those from  $k+1$  to  $A$  belong to quasi cluster(s). Here,  $\Lambda$  is a control parameter introduced for the single particle wave functions which belong to the quasi-cluster(s), and  $R$  is a distance parameter between the quasi cluster and center of mass of other clusters (which will be introduced later).

The preliminary A-particle wave function  $\Psi(\vec{r}_1, \dots, \vec{r}_A; \Lambda, R)$  depends upon a collective parameters or generator coordinates,  $\Lambda$  and  $R$ . The collective wave function,  $f(\Lambda, R)$ , is folded into  $\Psi$  to produce a system wave function that depends only on the nucleonic coordinates  $\vec{r}_i$ . The collective parameter  $\Lambda$  and  $R$  generate the trial A-particle wave function but disappears in the final state function  $\Phi(\vec{r}_1, \dots, \vec{r}_A)$ . For a given A-particle Hamiltonian, the projected GCM trial wave function (8) is then expressed with respect to the generator function  $f(\Lambda, R)$ .

### III. RESULTS

In this section, we investigate the cluster-shell competition due to the spin-orbit interaction using the GCM on a collective basis generated by the AQC basis states. The GCM studies will be applied in Sect. III.A for low-lying states of  $^{20}\text{Ne}$ , described as  $^{16}\text{O}$ -core and one quasi- $\alpha$  cluster, and in Sect. III.B for states of  $^{24}\text{Mg}$  given by  $^{16}\text{O}$ -core and two quasi- $\alpha$  clusters.

#### A. $^{20}\text{Ne}$

Numerous calculations exist for  $^{20}\text{Ne}$  within the model space of  $^{16}\text{O}+\alpha$  or  $^{12}\text{C}+\alpha+\alpha$  [40–42]. From the SM point of view, two protons (two neutrons) outside of the  $^{16}\text{O}$  core occupy the  $\pi(d_{5/2})$  ( $\nu(d_{5/2})$ ) orbit, and the spin-orbit interaction acts strongly [43, 44]. This effect cannot be taken into account in a simple cluster-model space. Hence, the hybrid models [45, 46] and the AMD approach [47, 48] have been applied to describe both the cluster structures and the single-particle motion of nucleons around the  $^{16}\text{O}$ -core. Finally, the  $^{16}\text{O}$ -core+ $3N+N$  three-cluster approach has been proposed to account for the breaking of one  $\alpha$ -cluster due to the spin-orbit interaction [49].

In our model of  $^{20}\text{Ne}$ , four  $\alpha$ -clusters form a tetrahedron which corresponds to the doubly closed  $p$ -shell if the relative distance between clusters is equal to zero. The actual distance between  $\alpha$ -clusters in the  $^{16}\text{O}$ -tetrahedron is 1.0 fm, and its center of mass is placed at the origin of the coordinate system. The remaining (quasi)- $\alpha$  cluster is located on the  $x$ -axis. The center of mass of this cluster is denoted by  $R\vec{e}_x$ , where  $R$  is a distance parameter and  $\vec{e}_x$  is the unit vector on the  $x$ -axis.

If the spin-orbit interaction acts, the quasi- $\alpha$  cluster has  $S \neq 0$  because the spatial part of the wave function for each nucleon of the quasi-cluster is not an eigenstate of the time-reversal operator. The dissolution of  $\alpha$ -

cluster ( $S = 0$ ) by the spin-orbit interaction is described by the control parameter (the generator coordinate)  $\Lambda$  in the AQC basis wave function. Since the direction of the spin is defined along the  $z$ -axis, we change the Gaussian centers of the nucleons in the quasi-cluster from  $R\vec{e}_x$  to  $R(\vec{e}_x + i\Lambda\vec{e}_y)$  or  $R(\vec{e}_x - i\Lambda\vec{e}_y)$ , for spin-up or spin-down nucleons, respectively, to assure that the directions of the spin and orbital parts of the angular momentum are parallel. Hence, the generalized center parameters of the quasi- $\alpha$  packet become:

$$\vec{\zeta}/\sqrt{\nu} = R(\vec{e}_x + i\Lambda\vec{e}_y) \quad , \quad (11)$$

and

$$\vec{\zeta}/\sqrt{\nu} = R(\vec{e}_x - i\Lambda\vec{e}_y) \quad , \quad (12)$$

for the for the spin-up and spin-down nucleons (proton or neutron), respectively. Here,  $R\vec{e}_x$  is the spatial position of the Gaussian center. Imaginary parts:  $R\Lambda\vec{e}_y$  and  $-R\Lambda\vec{e}_y$ , express the momenta of nucleons, and  $\vec{e}_x$  and  $\vec{e}_y$  are unit vectors on  $x$  and  $y$  axes, respectively.

These imaginary parts of the generalized center parameters of the quasi- $\alpha$  packet allow to mimic spherical harmonics with a parametrization (3). The spatial part of the single-particle wave function (3) of a nucleon in the quasi cluster is:

$$\psi_i = \left(\frac{2\nu}{\pi}\right)^{\frac{3}{4}} \exp[-\nu\vec{r}^2 - \vec{\zeta}^2 + 2\nu\vec{r} \cdot \vec{\zeta}/\sqrt{\nu}] \quad . \quad (13)$$

The last term can be expanded using (11), (12). In the case of a spin-up nucleon, for example, one obtains:

$$\exp[2\nu\vec{r} \cdot \vec{\zeta}/\sqrt{\nu}] = 1 + \sum_{k=1}^{\infty} \frac{1}{k!} (2\nu R(x + i\Lambda y))^k \quad . \quad (14)$$

For  $\Lambda = 1$ , one finds:

$$\exp[2\nu\vec{r} \cdot \vec{\zeta}/\sqrt{\nu}] = 1 + \sum_{k=1}^{\infty} \frac{1}{k!} \frac{1}{s_k} (2\nu r R)^k Y_{kk}(\Omega) \quad , \quad (15)$$

where  $s_k$  are the normalization factors of spherical harmonics  $Y_{kk}(\Omega)$ . Hence, the spatial part of the wave function of a spin-up nucleon in the quasi cluster can be written as:

$$\begin{aligned} \psi_i = \left(\frac{2\nu}{\pi}\right)^{\frac{3}{4}} \{ & 1 + s_1^{-1} 2\nu r_i R Y_{11}(\Omega_i) \\ & + (1/2!) s_2^{-1} (2\nu r_i R)^2 Y_{22}(\Omega_i) \\ & + (1/3!) s_3^{-1} (2\nu r_i R)^3 Y_{33}(\Omega_i) \\ & + \dots + (1/n!) s_n^{-1} (2\nu r_i R)^n Y_{nn}(\Omega_i) \\ & + \dots \} \exp[-\nu r_i^2] . \end{aligned} \quad (16)$$

Since the direction of spin is along the  $z$ -axis, the spin-up wave function is described as a linear combination of  $|j \ j_z = +j\rangle$  states:

$$\begin{aligned} & a_{1/2,1/2} |1/2 \ 1/2\rangle + a_{3/2,3/2} |3/2 \ 3/2\rangle \\ & + a_{5/2,5/2} |5/2 \ 5/2\rangle + \dots \quad . \end{aligned}$$

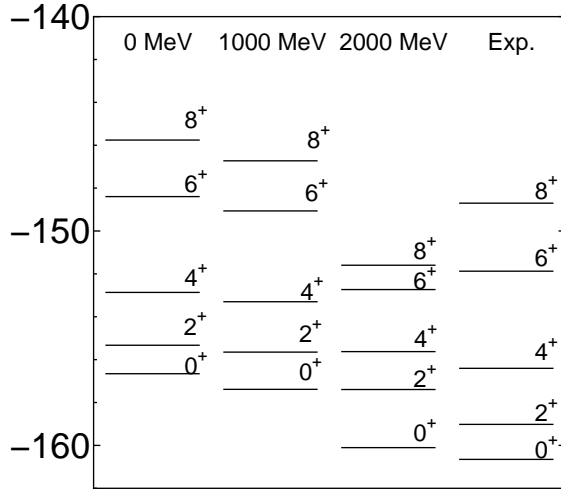


FIG. 1: The GCM calculations of yrast levels in  $^{20}\text{Ne}$  for three different values of the strength of the spin-orbit interaction:  $V_0 = 0, 1000, 2000$  MeV, are compared with the experimental data (Exp.). For more details, see the description in the text.

Analogously, the spatial part of the wave function for a spin-down nucleon is:

$$a_{1/2,-1/2}|1/2 - 1/2\rangle + a_{3/2,-3/2}|3/2 - 3/2\rangle + a_{5/2,-5/2}|5/2 - 5/2\rangle + \dots$$

This can be obtained by a time-reversal transformation of the spin-up wave function.

It is important to mention that all components of the quasi cluster wave function which overlap with the wave function of the core nucleus are exactly removed by the Pauli principle. In the case of  $^{20}\text{Ne}$ , four nucleons of the quasi cluster are excited to the  $sd$ -shell. For small  $R$ , the radial wave function for the spin-up proton/neutron corresponds to the  $r^2 Y_{22} \exp[-\nu r^2]$  SM wave function, whereas for the spin-down proton/neutron one finds  $r^2 Y_{2-2} \exp[-\nu r^2]$  SM radial wave function. Therefore,  $\Lambda$  is a parameter which can be used to characterize the cluster-shell competition:  $\Lambda = 1$  is a limit of the spherical harmonics, and  $\Lambda = 0$  is the  $\alpha$ -cluster limit. If  $R$  is large, the radial wave function contains admixtures of the higher shell components.

After setting Gaussian center parameters of nucleons in quasi cluster and  $\alpha$ -clusters, the whole system is Galilei transformed so that the center of gravity coincides with the origin of the coordinate system.

Fig. 1 shows energies of yrast states in  $^{20}\text{Ne}$ . We superpose basis states with different values of  $\Lambda$  ( $\Lambda = -1, -0.5, 0, 0.5, 1.0, 1.5, 2, 2.5, 3$ ) and  $R$  ( $R = 0.5, 1, 2, 3, 4$  fm) generator coordinates, and then diagonalize the Hamiltonian in this subspace. In this calculation, the Majorana parameter is  $M = 0.62$  and the size of the Gaussian wavepacket equals  $b = 1.6$  fm ( $b \equiv 1/\sqrt{2\nu}$ ). For this choice of the parameters, one can reproduce the binding energy of  $^{20}\text{Ne}$  reasonable well. The results with the strength of the spin-orbit interaction of  $V_0 = 0, 1000$ , and  $2000$

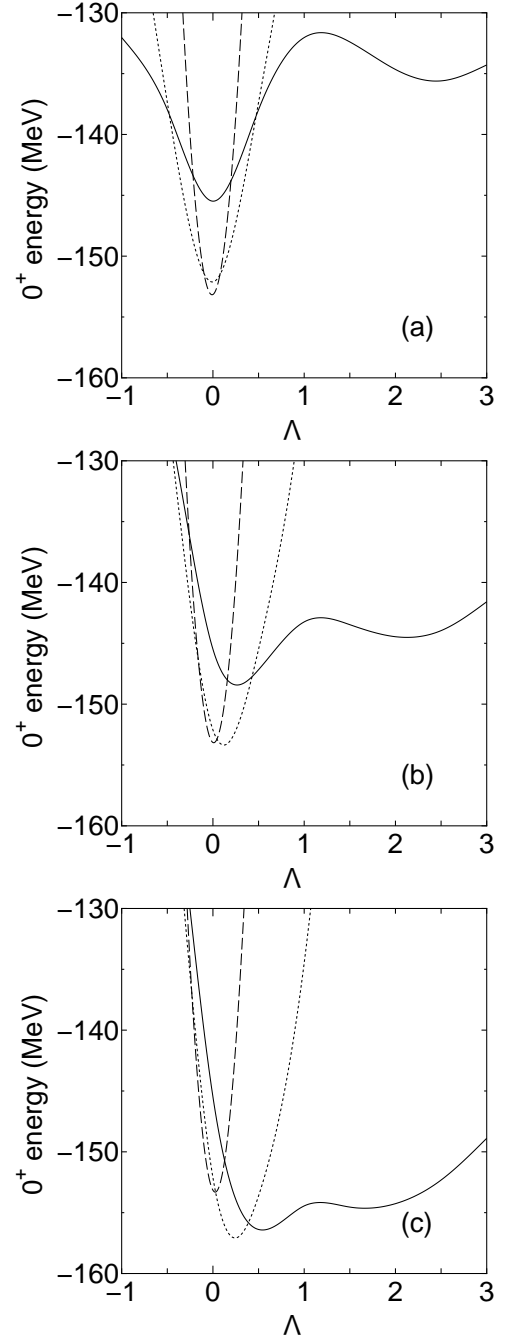


FIG. 2: The energy curves of the  $0^+$  state of  $^{20}\text{Ne}$  as a function of  $\Lambda$ : (a):  $V_0 = 0$  MeV, (b):  $V_0 = 1000$  MeV, and (c):  $V_0 = 2000$  MeV. The solid, dotted, and dashed lines show  $R = 0.5, 2$ , and  $4$  fm, respectively.

MeV are compared with experimental one (Exp.). The experimental level spacing among  $0^+, 2^+, 4^+$  shows the deviation from the  $l(l+1)$  rule for the rigid rotor, and the spin-orbit interaction is needed to explain this deviation; the experimental  $0^+ - 2^+$  level spacing is larger than the results with  $V_0 = 0$  MeV even if the  $0^+ - 4^+$  spacing is almost reproduced. It has been known that introducing the spin-orbit strength of  $V_0 = 2000$  MeV gives reason-

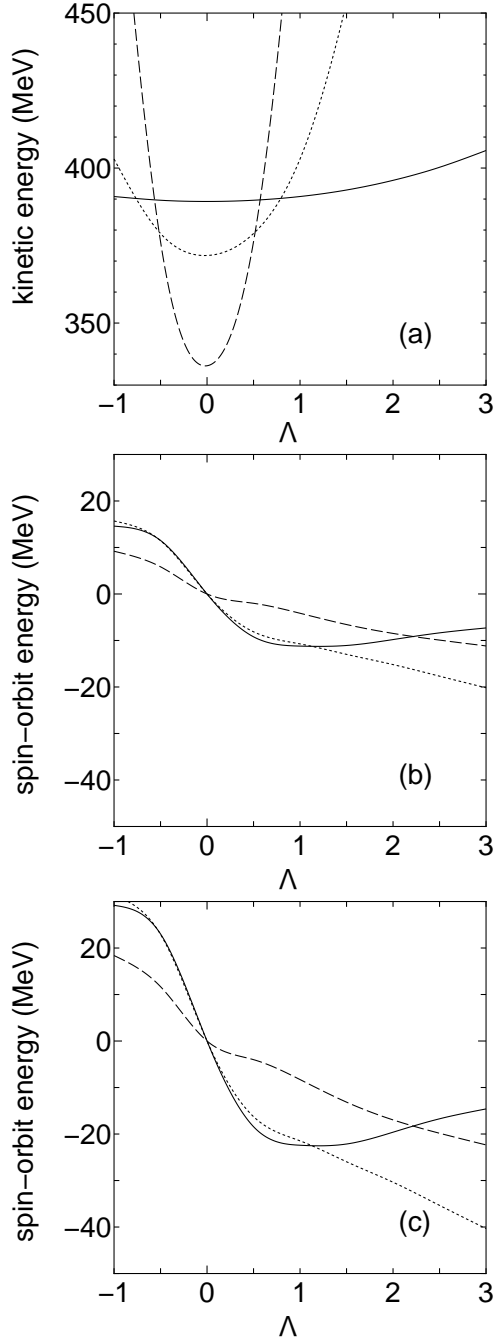


FIG. 3: The kinetic and spin-orbit energy curves of the  $0^+$  state of  $^{20}\text{Ne}$  as a function of  $\Lambda$ : (a): kinetic energy (independent of the spin-orbit strength), (b): spin-orbit energy for  $V_0 = 1000$  MeV, and (c): spin-orbit energy  $V_0 = 2000$  MeV. The lines are the same as in Fig. 2.

able description for the scattering phase shift of  $\alpha+N$ , however this strength is too strong for  $^{20}\text{Ne}$  judging from the obtained level spacing between the ground  $0^+$  state and  $8^+$  state. Therefore, the strength of  $V_0 = 1000$  MeV is considered to be the best to reproduce both the  $0^+ - 2^+ - 4^+$  and  $0^+ - 8^+$  level spacings. Both the experimental result and the calculation show that the  $8^+$

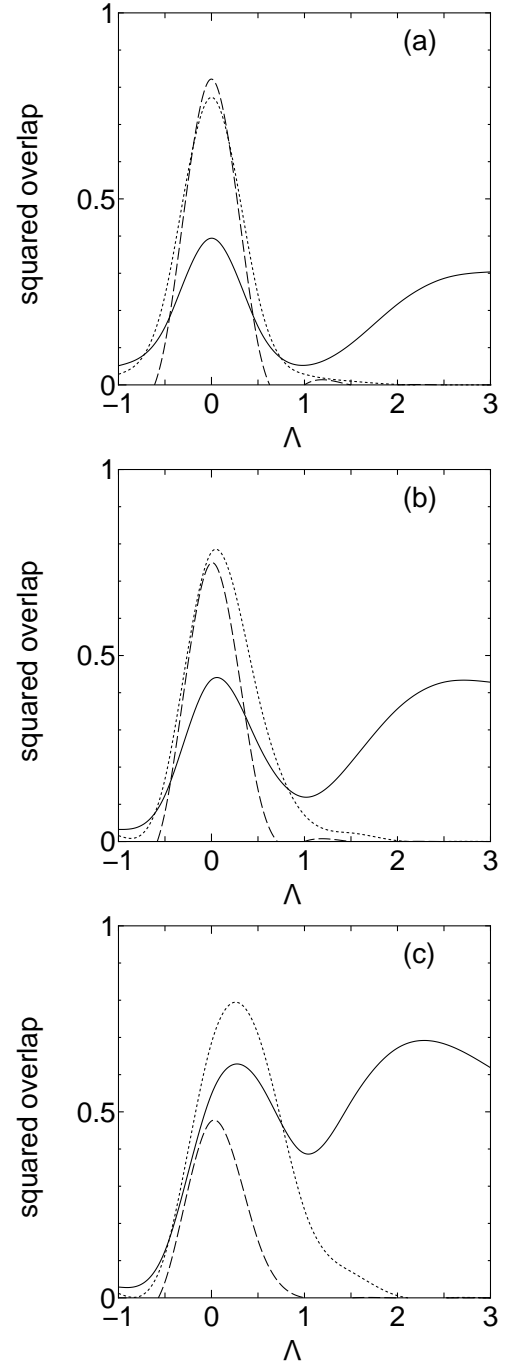


FIG. 4: The squared overlap between the lowest  $0^+$  state of  $^{20}\text{Ne}$  obtained by superposing the basis states with different  $R$  and  $\Lambda$  values and each basis state. (a):  $V_0 = 0$  MeV, (b):  $V_0 = 1000$  MeV, and (c):  $V_0 = 2000$  MeV. The lines are the same as in Fig. 2.

state does not fit to the sequence of the rotational band structure. This is due to the shell effect, and the deviation becomes larger with increasing the strength of the spin-orbit interaction.

One of the possible reasons why  $V_0 = 2000$  determined from the  $\alpha+N$  scattering is too strong for  $^{20}\text{Ne}$  is the

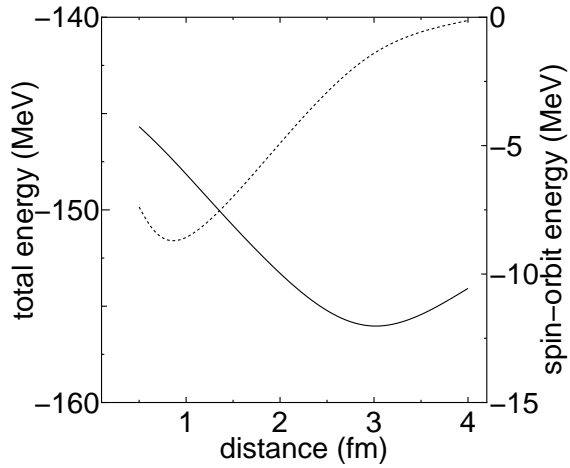


FIG. 5: The energy curves of the  $0^+$  state as a function of the distance between “quasi cluster” and  $^{16}\text{O}$  is shown. The solid line is total energy (left vertical axis), and the dotted line is spin-orbit energy (right vertical axis). The strength of the spin-orbit interaction is  $V_0 = 1000$  MeV, which gives reasonable level spacing in Fig. 1.

contribution of the tensor interaction. It has been known that the tensor interaction causes the two-particle-two-hole excitation of  $^4\text{He}$  from the  $(0s)^4$  configuration and this effect plays an essential role for explaining the spin-orbit splitting of  $^5\text{He}$  [50, 51]. Thus we somehow overestimate the spin-orbit strength when we try to fit the scattering phase shift of  $^4\text{He}+N$  using  $(0s)^4$  configuration for  $^4\text{He}$  and without introducing the tensor interaction explicitly. Also, the first order term of the tensor interaction (between  $j$ -upper protons and  $j$ -upper neutrons) acts repulsively [52]. In the present case, an  $\alpha$ -cluster is broken to take into account the spin-orbit interaction, and two protons and two neutrons occupy the  $j$ -upper orbits, and the first order term of the tensor interaction acts repulsively between protons and neutrons. Renormalization of this tensor effect into the spin-orbit part is another reason for the reduction of the strength of the spin-orbit interaction.

The energy curves of the  $0^+$  state as a function of  $\Lambda$ , which are expressed as

$$\langle \Psi(\vec{r}_1, \dots, \vec{r}_A; \Lambda, R) | \hat{H} | \Psi(\vec{r}_1, \dots, \vec{r}_A; \Lambda, R) \rangle / \langle \Psi | \Psi \rangle$$

in terms of Eq. (9), are shown in Fig. 2, where (a):  $V_0 = 0$  MeV, (b):  $V_0 = 1000$  MeV, and (c):  $V_0 = 2000$  MeV. The lines are the results with different distance between  $^{16}\text{O}$  and quasi  $\alpha$ -cluster, and the solid, dotted, and dashed lines are cases of  $R = 0.5, 2$ , and  $4$  fm, respectively. In the case of  $V_0 = 0$  MeV ((a)), the minimum points of the curves appear around  $\Lambda = 0$ . This is because there is no spin-orbit interaction in this case. Introducing  $\Lambda$  value induces the rotation of four nucleons in the “quasi  $\alpha$ ” cluster around  $^{16}\text{O}$ , which increases the kinetic energy of the four nucleons. Thus, without spin-orbit interaction, the energy does not decrease. On the

other hand, with increasing the  $V_0$  value, the minimum points shift to finite  $\Lambda$  value ((b) and (c)). The lowest energy is obtained with  $R = 3$  fm and  $\Lambda \sim 0.2$  in the case of  $V_0 = 1000$  MeV (although the line for  $R = 3$  fm is not shown in this figure).

The kinetic and spin-orbit energy curves of the  $0^+$  state of  $^{20}\text{Ne}$  as a function of  $\Lambda$  are shown in Fig. 3, where (a): kinetic energy (independent of the spin-orbit strength), (b): spin-orbit energy for  $V_0 = 1000$  MeV, and (c): spin-orbit energy  $V_0 = 2000$  MeV. The lines are the same as in Fig. 2.

The squared overlap between the lowest  $0^+$  state of  $^{20}\text{Ne}$  obtained by superposing the basis states with different  $R$  and  $\Lambda$  values and each basis state, which is expressed as

$$|\langle \Psi(\vec{r}_1, \dots, \vec{r}_A; \Lambda, R) | \Phi(\vec{r}_1, \dots, \vec{r}_A) \rangle|^2 / \sqrt{\langle \Psi | \Psi \rangle \langle \Phi | \Phi \rangle}$$

in terms of Eqs. (8) and (9), is shown in Fig. 4 ((a):  $V_0 = 0$  MeV, (b):  $V_0 = 1000$  MeV, and (c):  $V_0 = 2000$  MeV). Here, the lines are the same as in Fig. 2. Both the bra (each basis state on the horizontal axis) and ket (the lowest  $0^+$  state obtained after superposing the basis states) states are normalized, however, since the basis states with different  $\Lambda$  value are non-orthogonal, the integration over  $\Lambda$  does not correspond to definite physical value. It is shown that when the spin-orbit interaction is strong (in the case of (c)), the peak positions shift to the finite  $\Lambda$  values similarly to Fig. 2. This result suggests the mixing of two components (cluster limit and shell limit) in the ground state of  $^{20}\text{Ne}$ . Also, the height of the second peak for the solid line ( $R = 0.5$  fm) shown around  $\Lambda \sim 2$  increases with increasing strength of the spin-orbit interaction ((a)  $\rightarrow$  (b)  $\rightarrow$  (c)). The states with  $\Lambda$  larger than 1 surely correspond to particle-hole excitation to higher shells, however physical interpretation for it is still an open question.

In Fig. 5, the energy curves of the  $0^+$  state as a function of the distance between “quasi cluster” and  $^{16}\text{O}$  is shown (solid line: total energy, dotted line: spin-orbit energy). Here, the strength of the spin-orbit interaction is  $V_0 = 1000$  MeV, which gives reasonable level spacing in Fig. 1. The optimal  $\Lambda$  value is chosen at each point on the horizontal axis. It is shown that the energy becomes minimum around the distance of 3 fm, where the contribution of the spin-orbit interaction is  $\sim -2.5$  MeV, and the expectation value of the spin-orbit interaction increases to  $\sim -8$  MeV in the inner region.

The energy curves of (a)  $2^+$ , (b)  $4^+$ , (c)  $6^+$ , and (d)  $8^+$  states as a function of  $\Lambda$  are shown in Fig. 6. The solid, dotted, and dashed lines show the results of  $R = 0.5, 2$ , and  $4$  fm, respectively. Here, the strength of the spin-orbit interaction is  $V_0 = 1000$  MeV, which gives reasonable level spacing in Fig. 1. With increasing angular momentum the optimal  $R$  value gets shorter, and the minimum energy of the dashed line ( $R = 4$  fm) rapidly increase compared with the solid and dotted lines in high angular momentum states. Also, the optimal  $\Lambda$  value increases with increasing angular momentum.

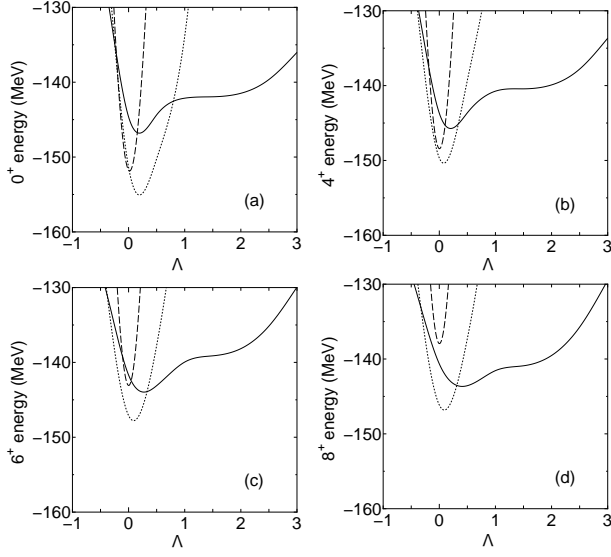


FIG. 6: The energy curves of (a)  $2^+$  (b)  $4^+$  (c)  $6^+$  and (d)  $8^+$  states as a function of  $\Lambda$ . The lines are the same as in Figs. 2, 3, 4. The strength of the spin-orbit interaction is chosen to be  $V_0 = 1000$  MeV.

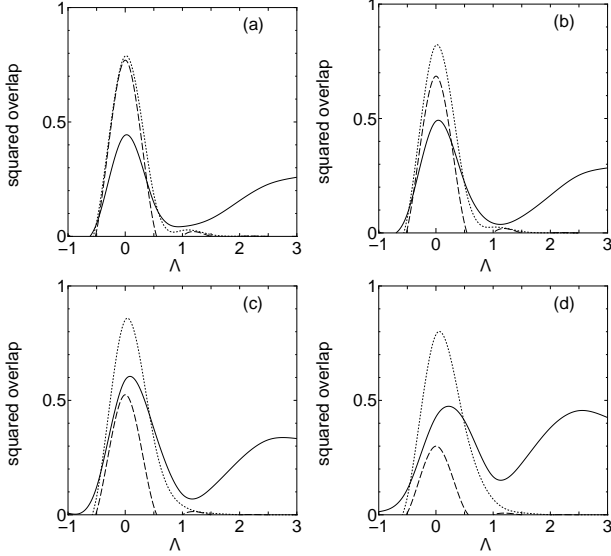


FIG. 7: The squared overlap between the lowest (a)  $2^+$  (b)  $4^+$  (c)  $6^+$  and (d)  $8^+$  states obtained by superposing the basis states with different  $R$  and  $\Lambda$  values and each basis state. The lines are the same as in Figs. 2, 3, 4, 6. The strength of the spin-orbit interaction is chosen to be  $V_0 = 1000$  MeV.

The squared overlap between the obtained (a)  $2^+$ , (b)  $4^+$ , (c)  $6^+$ , and (d)  $8^+$  states by superposing the basis states with different  $R$  and  $\Lambda$  values and each basis state is shown in Fig. 7. The lines are the same as in Figs. 2, 3, 4, 6. The strength of the spin-orbit interaction is chosen to be  $V_0 = 1000$  MeV. With increasing angular momentum, the height of the dashed line ( $R = 4$  fm) decreases and the  $R$  value which gives the largest overlap

gets shorter, similarly to Fig. 6. Also, the  $\Lambda$  value which gives the largest overlap slightly increases with increasing angular momentum.

We can apply the present method also for the negative parity states. However, it is known that the cluster structure is really important for the lowering of the higher nodal states like the negative parity states. Thus the  $\alpha$  breaking effect plays a less important role for the negative parity states. If we include the  $\alpha$  breaking wave functions (finite  $\Lambda$  values) in the model space, the energy gain for the  $1^-$  state of  $^{20}\text{Ne}$  (the band head of the negative parity band) is only 0.3 MeV with respect to the pure cluster model configuration, for the spin-orbit interaction strength  $V_0 = 1000$  MeV. This energy gain becomes 0.8 MeV for  $V_0 = 2000$  MeV, what is anyway much smaller than in the case of the positive parity states.

## B. $^{24}\text{Mg}$

Next we discuss the case with two quasi clusters around the  $^{16}\text{O}$  core, that is  $^{24}\text{Mg}$ . In the previous case of  $^{20}\text{Ne}$ , one quasi cluster is placed on the  $x$ -axis and four nucleons in this quasi cluster are changed to  $Y_{22}$  (proportional to  $(x+iy)^2/r^2$ ) or  $Y_{2-2}$  (proportional to  $(x-iy)^2/r^2$ ) orbitals after giving the imaginary part in the  $y$  component. In  $^{24}\text{Mg}$ , the second quasi cluster should be transformed to  $Y_{21}$  and  $Y_{2-1}$  for spin-up and spin-down nucleons, respectively, to make the orbital and spin components parallel. The spherical harmonics  $Y_{21}$  ( $Y_{2-1}$ ) is proportional to  $(x+iy)z/r^2$  ( $(x-iy)z/r^2$ ), and it is necessary to shift the Gaussian center parameters of nucleons in quasi clusters also to  $z$  direction.

For the first quasi cluster, we give the Gaussian centers parameter

$$\vec{\zeta}_1/\sqrt{\nu} = R(\vec{e}_x + i\Lambda\vec{e}_y + \vec{e}_z/2) \quad (17)$$

for the spin-up proton and neutron, and

$$\vec{\zeta}_1/\sqrt{\nu} = R(\vec{e}_x - i\Lambda\vec{e}_y + \vec{e}_z/2) \quad (18)$$

for the spin-down proton and neutron. For the second quasi cluster, we give

$$\vec{\zeta}_2/\sqrt{\nu} = R(\vec{e}_x + i\Lambda\vec{e}_y - \vec{e}_z/2). \quad (19)$$

for the spin-up proton and neutron and

$$\vec{\zeta}_2/\sqrt{\nu} = R(\vec{e}_x - i\Lambda\vec{e}_y - \vec{e}_z/2) \quad (20)$$

for the spin-down proton and neutron, where  $\vec{e}_x$ ,  $\vec{e}_y$ , and  $\vec{e}_z$  are unit vectors. The antisymmetrization effect allows us to take linear combinations of orbitals for the first and the second quasi clusters: when the linear combination is in-phase

$$\exp[-\nu(\vec{r} - \vec{\zeta}_1/\sqrt{\nu})^2] + \exp[-\nu(\vec{r} - \vec{\zeta}_2/\sqrt{\nu})^2], \quad (21)$$



there is no node in the  $z$  direction, however when it is anti-phase,

$$(\exp[-\nu(\vec{r} - \vec{\zeta}_1/\sqrt{\nu})^2] - \exp[-\nu(\vec{r} - \vec{\zeta}_2/\sqrt{\nu})^2])/R, \quad (22)$$

factor  $z$  is multiplied and one node in the  $z$  direction appears at the limit of  $R \rightarrow 0$ . When we expand the exponents of Eqs. (21) and (22), similar discussion to Eqs. (13) – (16) follows. Here the components of  $0s$  and  $p$  shells disappear due to the presence of the  $^{16}\text{O}$  core. Eventually proton and neutron that occupy a state of Eq. (21) correspond to  $Y_{22}$  (spin-up case) and  $Y_{2-2}$  (spin-down case) the same as in the  $^{20}\text{Ne}$  case, however proton and neutron that occupy a state of Eq. (22) correspond to  $Y_{21}$  (spin-up case) and  $Y_{2-1}$  (spin-down case) due to the factor “ $z$ ”. After setting all these Gaussian center parameters, the whole system is Galilei transformed so that the center of gravity coincides with the origin of the coordinate system.

The energy curves for the  $0^+$  state of  $^{24}\text{Mg}$  as a function of  $\Lambda$  are shown in Fig. 8, where (a):  $V_0 = 0$  MeV, (b):  $V_0 = 1000$  MeV, and (c):  $V_0 = 2000$  MeV. In Fig. 8 (a), the energy minima are shown around  $\Lambda = 0$  independent of  $R$ , however states with finite  $\Lambda$  values become important especially for lines with small  $R$  in Figs. 8 (b) and 8 (c) with increasing spin-orbit strength. In Fig. 8 (b), the second minimum point appears around  $\Lambda = 1.5$  for the solid line ( $R = 0.5$  fm), and two local minima of the solid line in Fig. 8 (b) merge into a deep minimum point in Fig. 8 (c).

The squared overlap between the lowest  $0^+$  state of  $^{24}\text{Mg}$  obtained by superposing the basis states with different  $R$  and  $\Lambda$  values and each basis state is shown in Fig. 9 ((a):  $V_0 = 0$  MeV, (b):  $V_0 = 1000$  MeV, and (c):  $V_0 = 2000$  MeV). Here, the lines are the same as in Fig. 8. it is again shown that when the spin-orbit interaction is strong (in the case of (c)), the peak positions shift to the finite  $\Lambda$  values similarly to Fig. 4. This result suggests the mixing of two components (cluster limit and shell limit) in the ground state of  $^{24}\text{Mg}$ . Also, the height of the second peak for the solid line ( $R = 0.5$  fm) shown around  $\Lambda \sim 2$  increases with increasing strength of the spin-orbit interaction ((a)  $\rightarrow$  (b)  $\rightarrow$  (c)).

TABLE I: The ground state energy of  $^{24}\text{Mg}$  calculated with the strength of the spin-orbit interaction,  $V_0 = 0$ , 1000, and 2000 MeV. The results of one and two generator coordinate(s) are compared.

$V_0$	one generator coordinate	two generator coordinates
0	-189.8	-190.1
1000	-190.9	-191.4
2000	-196.8	-198.2

For more precise calculation, we can introduce two generator coordinates; the relative distance between the two quasi clusters ( $R_1 = 0.5, 1.0, 2.0, 3.0$  fm) and the relative distance between the center of mass of two quasi clusters and the  $^{16}\text{O}$  core ( $R_2 = 0.5, 1.0, 2.0, 3.0$  fm).

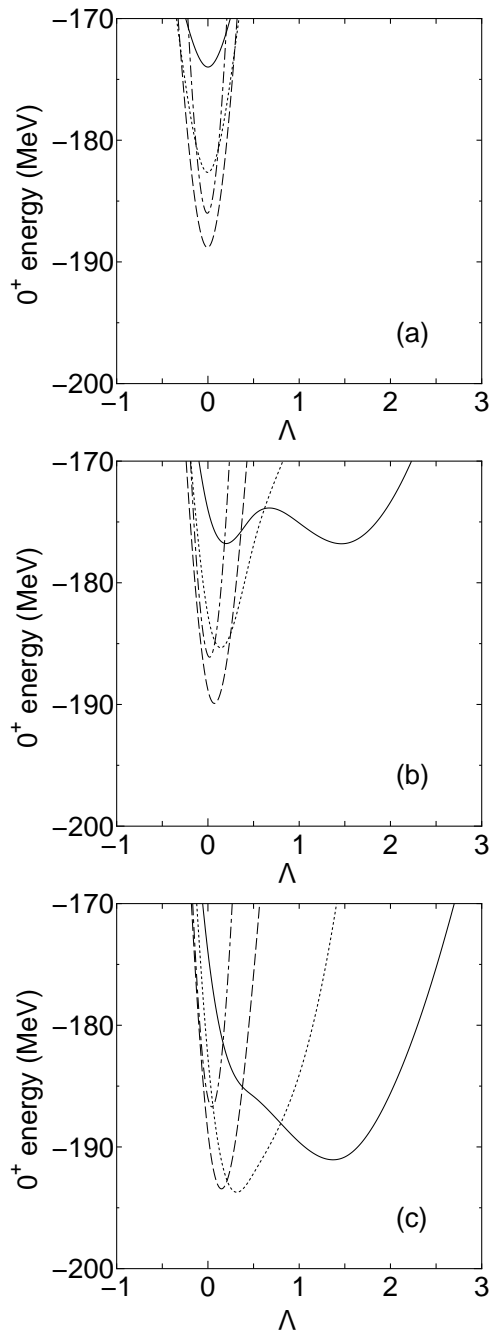


FIG. 8: The energy curves for the  $0^+$  state of  $^{24}\text{Mg}$  as a function of  $\Lambda$ : (a):  $V_0 = 0$  MeV, (b):  $V_0 = 1000$  MeV, and (c):  $V_0 = 2000$  MeV. The solid, dotted, dashed, and dash-dotted lines show  $R = 0.5, 1, 2$ , and  $3$  fm, respectively.

The result of the ground state ( $0^+$ ) energy as a function of the strength of the spin-orbit interaction ( $V_0$  in Eq. (7)) is shown in Table I (in the column of two generator coordinates), together with the results of one generator coordinate ( $R$ ). Here, the difference between the results of  $V_0 = 0$  MeV and  $V_0 = 2000$  MeV is 8.2 MeV in the case of two generator coordinates. The effect of the decrease of energy due to the spin-orbit interaction is dou-

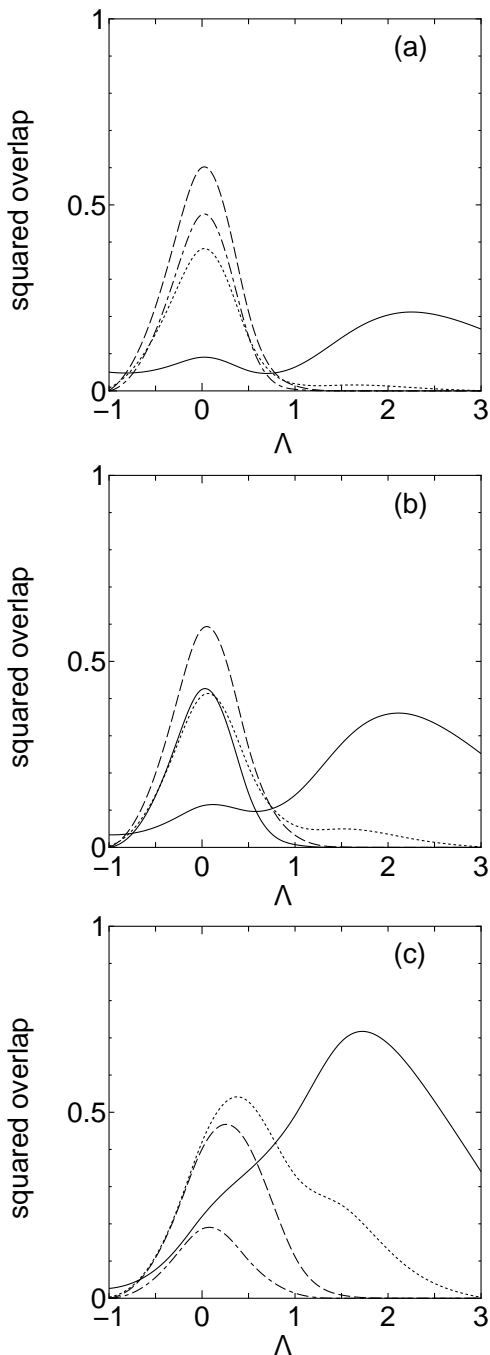


FIG. 9: The squared overlap between the lowest  $0^+$  state of  $^{24}\text{Mg}$  obtained by superposing the basis states with different  $R$  and  $\Lambda$  values and each basis state. (a):  $V_0 = 0$  MeV, (b):  $V_0 = 1000$  MeV, and (c):  $V_0 = 2000$  MeV. The lines are the same as in Fig. 8.

bled compared with  $^{20}\text{Ne}$  (Fig. 1), since we have broken two  $\alpha$  clusters in  $^{24}\text{Mg}$ .

#### IV. A POSSIBLE CONNECTION TO GROUP THEORETICAL APPROACHES

In this section we discuss how a similar study could be formulated in terms of group theoretical models, in order to investigate the possible phase-transitions from a different angle and in a more quantitative way. A reasonable approach would consist of two steps. The first one is the algebraic cluster model calculation, and the second step is the shell-model calculation. The two parts have a matching point: the  $U(3)$  dynamical symmetry is present in both models [29].

##### A. Basic features of the group theoretical investigations

The basic features of the algebraic studies can be summarized as follows. A group-theoretical model is considered with a well-defined model space. On the other hand the interactions (but only the interactions) are varied. They have limiting cases, called dynamical symmetries. When a dynamical symmetry holds, the eigenvalue-problem has an analytical solution, due to the fact that the Hamiltonian can be expressed in terms of the invariant operators of a chain of nested subgroups. In such a case the eigenstates of the Hamiltonian have a complete set of good quantum numbers. The general Hamiltonian, however, which has contributions from interactions with different dynamical symmetries, has to be diagonalized numerically. The relative weight of the dynamically symmetric limits serves as a control parameter, and it defines the phase-diagram of the system. When there are more than two dynamical symmetries, more than one control parameters appear.

In the limit of large particle number phase-transitions are seen in the sense that the derivative of the energy-minimum, as a function of the control-parameter, is discontinuous. The order of the derivative, showing the discontinuity, gives the order of the phase-transition. Thus, in this framework the phase-transition is investigated quantitatively, like in the thermodynamics. A phase is defined as a region of the phase diagram between the endpoint of the dynamical symmetry and the transition point. It is also conjectured [53] that such a quantum phase is characterized by a quasi-dynamical symmetry. Therefore, although the real dynamical symmetry is valid only at a single point of the phase-diagram, the more general quasi-dynamical symmetry may survive, and in several cases does survive [29, 53], in the whole phase. If this conjecture really turns out to be true, then the situation is similar to Landau's theory: different phases are determined by different (quasi-dynamical) symmetries, and phase transitions correspond to a change of the symmetry.

In the case of the finite particle number the discontinuities are smoothed out, as the consequence of the finite size effect, but still remarkable changes can be detected

in the behavior of the corresponding functions.

In this paper we have investigated the cluster-shell competition by enlarging the cluster-model-space with some shell-model basis states. The shell-model description, in general, is based on a horizontal truncation of the model space (e.g. to a single major shell), while the cluster model makes a vertical truncation (e.g. a few nucleons with specific symmetry in many major shells). Therefore, a model space containing both subspaces, and being a space for an irreducible representation of a dynamical algebra can be prohibitively large. Thus, the formulation of the cluster-shell competition in terms of the group theoretical framework seems to be feasible in a two-step procedure. The first step is the cluster study based on an algebraic model, the second one is the shell-model calculation. The reason why they can be combined to a coherent investigation is that they have a matching point: both of them have a limit of the  $U(3)$  dynamical symmetry [29].

### B. $U(3)$ limit in the algebraic cluster model

We begin with the algebraic cluster model. In case of a binary cluster-configuration of closed-shell clusters, e.g.  $^{16}\text{O}+^4\text{He}$ , we practically need to describe only the relative motion. Algebraically it can be done by applying the vibron model of  $U(4)$  structure [54], which have  $(l=1)$   $\pi$  and  $(l=0)$   $\sigma$  bosons, as building blocks. The Pauli-principle can be taken into account by a basis-truncation in the simple case of closed-shell clusters [55], and with this constraint the vibron model can really give a reasonable approach to the  $\alpha$ -cluster bands of  $^{20}\text{Ne}$  [56].

The  $U(4)$  algebra of the relative motion can be considered as the dynamical algebra of the truncated harmonic oscillator problem for a finite spectrum (as the compact form of the noncompact  $U(3,1)$  dynamical algebra of the oscillator problem without truncation). It is worth stressing here that this simplified algebraic structure is valid only from the viewpoint of the physical operators when no coupling to the internal cluster degrees of freedom is considered. From the viewpoint of the model space, on the other hand, the internal degrees of freedom have to be taken into account, otherwise the Pauli-principle could not be appreciated [55]. The internal cluster structure is usually described in terms of the Elliott-model of  $U_c^{ST}(4) \otimes U_c(3)$  group structure, where  $U_c^{ST}(4)$  refers to the spin-isospin degrees of freedom and  $U_c(3)$  stands for the space-part of the internal cluster wave function.

The cluster model with the  $U(4)$  algebraic structure has two dynamical symmetries:  $U(3)$ , and  $O(4)$ . Therefore, the phase-space is one-dimensional, having these limits as ending points. The  $U(3)$  limit corresponds to a soft vibrator in the language of the collective model, or to a shell-model-like clusterization from the microscopic viewpoint. The  $O(4)$  represents the rigid rotor limit, i.e. a rigid molecule-like configuration, which extends to very many major shells [22]. A recent schematic calculation

[57] showed that at a certain value of the control parameter a phase-transition takes place, and the quasidynamical  $U(3)$  symmetry characterizes the whole phase from the limit of the real dynamical symmetry up to very close to the point of transition.

When the coupling between the relative motion and internal cluster degrees of freedom is taken into account [55], then there is a third dynamical symmetry of the cluster model, denoted by  $SO(3)$ , which corresponds to the weak-coupling limit. Then the phase diagram is two dimensional, and can be illustrated by a triangle [29].

### C. $U(3)$ limit in the shell model

The  $U(3)$  symmetry is known to be very important in the shell model since the pioneering work of Elliott [58]. A specific  $U(3)$  symmetry defines a (collective) rotational band in terms of the basis of the spherical shell model. (In the shell-model context the symmetry is usually called  $SU(3)$ , and not  $U(3)$ ). The two groups are uniquely related to each other, once the total number of particles (oscillator quanta) is given, this being the only extra generator of  $U(3)$  in comparison with  $SU(3)$ . In the shell model calculations usually only a single major shell is incorporated, therefore, this number does not play any role, and it is not needed. In the cluster model, however, several major shells are included, thus it is more practical to use  $U(3)$ , which defines  $SU(3)$ , too.)

The problem of a shell-model-like phase-transition has been studied in [59]. This is also a schematic calculation, in which a finite fermion system was considered, with a Hamiltonian having two dynamical symmetries: the  $SU(3)$  one of the Elliott model, and the  $SU(2)$  dynamical symmetry, which diagonalizes the pairing interaction of the superconductivity. A phase-transition was observed at a critical point of the control parameter, and the quasi-dynamical  $SU(3)$  symmetry turned out to be valid between the transition point and the endpoint of the  $SU(3)$  limit.

From the viewpoint of the phase studies it is remarkable that recently a triangle-like phase diagram has been proposed also for the shell model [60], which, in addition to the  $SU(3)$  and  $SU(2)$  symmetries has the independent-particle model as the third corner.

As the realistic calculations are concerned, the method of the works [61] are especially remarkable from our viewpoint. There the  $^{20}\text{Ne}$  was described within a shell-model, by considering 4 nucleons in the full sd shell, and applying  $SU(3)$  basis. The Hamiltonian includes spin-orbit, quadrupole-quadrupole and pairing terms as well.

### D. Matching of the two models at the $U(3)$ limit

The  $U(3)$  limit of the two (cluster and shell) models coincide with each other, as mentioned before, and will be discussed more in detail later on. The difference in the

physical content, as indicated here (vibrational limit in the cluster model and rotational limit in the shell model) seems to be a contradiction, but in fact it is not. In the shell model the  $U(3)$  dynamical symmetry determines a rotational band from the basis states of a single major shell. On the other hand the vibrational limit of the cluster model is related to major shell excitations. If the algebraic ( $U(3)$ ) shell model is extended by the inclusion of major shell excitations, then it has an algebraic structure of  $Sp(3, R)$  [62]. In the limit of the large particle number, however, it simplifies to a  $U(3)$  boson model [63], (or contracted symplectic model [64],) which contains both the hydrodynamic model (major shell excitations corresponding to giant resonances), and the Elliott  $SU(3)$  model. Similarly, the  $U(3)$  dynamical symmetry of the cluster model incorporates the major shell excitations as well as the  $SU(3)$  structure within the major shells [55]. (In the language of the liquid drop collective model, Elliott's  $SU(3)$  corresponds to the vorticity of the liquid: the (0,0)  $SU(3)$ -scalar represents the irrotational flow, while non- $SU(3)$ -scalar corresponds to non-zero vorticity.)

In this article we have introduced AQC model to describe the cluster-shell competition, where  $\Lambda$  and  $R$  are two parameters to characterize the state. We can map the values of  $\Lambda$  and  $R$  on the diagram in Fig. 10. The  $U(3)$  limit is characterized as small  $R$  and small  $\Lambda$ , thus the wave function has both natures of cluster and shell models. Increasing  $\Lambda$  changes  $\alpha$  cluster(s) to  $jj$ -coupling wave function, which corresponds to the shift of the wave function from the  $U(3)$  limit (common intersection) to the  $SU(2)$  limit on the shell model side, and increasing  $R$  corresponds to the change from the  $U(3)$  limit to the  $O(4)$  limit (rigid rotor state) on the cluster model side. In this way, AQC model can be interpreted in terms of the group theory by introducing a diagram in Fig. 10.

An algebraic study, which is similar to our present investigation of the cluster-shell competition would require two kinds of calculations. The first one is an extension of the work of Ref. [57] within the algebraic cluster study for the realistic description of the cluster band(s). This could determine quantitatively, where the real nucleus sits on the phase diagram of the cluster model. The  $U(3)$  end of this diagram is the common intersection with the phase diagram of the shell model. In particular, in the  $U(3)$  limit the cluster wave function of the ground state band of  $^{20}\text{Ne}$  e.g. is given by the shell-model wave function with the quantum numbers:  $U^{ST}(4) : [1, 1, 1, 1]$ ,  $S = 0$ ,  $T = 0$ ,  $U(3) : (8, 0)$ , i.e. the shell-model and cluster model wave functions are the same (apart from the normalization factor). The second part of the calculation should be a shell-model study, similar in spirit to those of [59, 61]. We discuss here the necessary scenario from the angle of the work [61]. i) Include not only the ground-band, but also the negative parity band, and ii) investigate the behavior of the system under the influence of the systematic change of the strength of the spin-orbit and/or pairing interactions. iii) When doing so the sur-

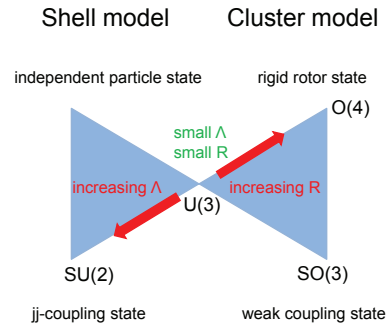


FIG. 10: (Color online) Schematic diagram for the group theoretical understanding for cluster-shell competition.

vival of the quasidynamical  $SU(3)$  could be determined from the analysis of the wave function.

The control parameter is the relative weight of the  $U(3)$  symmetry-breaking interaction in both cases. On the cluster side it is the dipole interaction (compared to the  $U(3)$ -symmetric quadrupole one), while on the shell-model side it can be spin-orbit and pairing forces. The quasi-dynamical  $U(3)$  symmetry defines a phase on both sides of real  $U(3)$  dynamical symmetry (being the matching point of the two phase-diagram). This kind of investigation could answer a question, like: where the system is located on the phase diagram of the cluster model and that of the shell-model. Furthermore, one could figure out if phase-transition(s) take(s) place, and if so, what kind of transitions.

## V. CONCLUSION AND FURTHER OUTLOOK

Recently, a microscopic calculation of the cluster-shell competition became possible, and in this work we introduced the GCM+AQC formalism to describe this competition in a simple way. The spin-orbit interaction is a key quantity which drives the transition from CM states to SM states. In our model, this effect is implanted into the trial wave function. By introducing a single parameter  $\Lambda$ , one  $\alpha$  cluster orbiting around  $^{16}\text{O}$  is changed into a “quasi cluster”, where the motion of four nucleons depends on the spin direction of each nucleon.

The energy levels of  $^{20}\text{Ne}$  calculated in the GCM on a collective basis of the AQC states for different strengths of the spin-orbit interaction:  $V_0 = 0, 1000, 2000$  MeV, were compared with the experimental data. The experimental level spacing of  $0^+ - 2^+ - 4^+$  shows a clear deviation from the  $l(l+1)$  rule, and the spin-orbit interaction is needed to explain this deviation. Although a reasonable description of the scattering phase shift in  $^4\text{He}+N$  reaction is possible for  $V_0 = 2000$  MeV, this value should be reduced for  $^{20}\text{Ne}$ . Judging from the level spacing between the ground state  $0^+$  and the  $8^+$  excited state, the optimal value of the spin-orbit coupling strength is

$V_0 = 1000$  MeV. Thus, the spin-orbit strength is overestimated if the scattering phase shift in  $^4\text{He}+N$  is fitted without introducing the tensor interaction explicitly. Both the experimental results and the GCM+AQC calculation show that the  $8^+$  state in  $^{20}\text{Ne}$  deviates strongly from the rotational sequence. Our studies demonstrate that the deviation increases with increasing the strength of the spin-orbit interaction.

For  $V_0 = 0$  MeV, the energy of a  $0^+$  state as a function of  $\Lambda$  exhibits a minimum at  $\Lambda = 0$ . With an increasing value of  $V_0$ , the minimum is shifted towards a finite value of  $\Lambda$  and the kinetic energy of nucleons in the  $\alpha$  quasi cluster increases as well. For  $V_0 = 1000$  MeV, the energy minimum is found at  $\Lambda \sim 0.2$ . The optimal value of  $\Lambda$  value increases with increasing the angular momentum.

The curves of energy as a function of  $\Lambda$  show that an optimal value of  $R$  (a distance between  $^{16}\text{O}$  and an  $\alpha$  quasi cluster) is around 3 fm for  $2^+$ . With increasing angular momentum, the optimal value of  $R$  decreases ( $R = 2$  fm for  $8^+$ ).

Furthermore, we discussed the case of two quasi clusters around the  $^{16}\text{O}$  core (the case of  $^{24}\text{Mg}$ ) showing the way two  $\alpha$  clusters can be broken in AQC formalism.

Concerning the three different kinds of states from the viewpoint of their shell or cluster nature: the SM states, the CM states and the SMC states, the following correspondence can be made in the language of the AQC formalism. The SM state (type (i)) corresponds to a situation of small  $R$  and large  $\Lambda$ , while a rigid molecule-like CM state (type (ii)) corresponds to large  $R$  and small  $\Lambda$ . The SMC state (type (iii)) involves small  $R$  and small  $\Lambda$  values. Usually,  $R$  is finite due to the Pauli exclusion principle. It follows from the present GCM+AQC study that even parity states of  $^{20}\text{Ne}$  and  $^{24}\text{Mg}$  are of the type (iii).

We have also discussed how a similar study could be formulated in terms of algebraic models. A possible approach would consist of two steps. The first one is the description of experimental data in terms of the algebraic

cluster model, and the second step is the shell-model calculation. The reason why they can be combined is that they have a matching point, the limit of the  $U(3)$  dynamical symmetry [29], which is the intersection of two phase-diagrams. The control parameter would be the relative weight of the  $U(3)$  symmetry-breaking interactions. Via this route, one might hope to understand whether the phase-transition possibly takes place between the cluster- and shell-configurations and what could be the nature of this transitions.

The  $U(3)$  symmetry is a common intersection of the cluster and shell models. CM and SM states can be characterized using the two triangles (see Fig. 10) which merge in the  $U(3)$  limit. In this paper, we have studied the cluster-shell competition using the GCM+AQC microscopic framework. In this framework,  $\Lambda$  and  $R$  are parameters of a collective AQC basis, which give an insight into the nature of many-body states. These parameters can be associated with features shown on this diagram. The  $U(3)$  limit is characterized by small  $R$  and small  $\Lambda$  values, thus the wave function has the nature of both cluster and shell models. Increasing  $\Lambda$  changes  $\alpha$  cluster(s) into  $jj$ -coupling wave function, which corresponds to the shift from  $U(3)$  to the  $SU(2)$  limit on the shell model side. Finally, increasing  $R$  corresponds to the change from  $U(3)$  to the  $O(4)$  limit (the rigid rotor state) on the cluster model side. In this way, the microscopic results of the GCM+AQC model can be interpreted in intuitive language of the group theory.

## Acknowledgments

One of the authors (N.I.) would like to thank JSPS Core-to-core program. This work was supported in part by the OTKA grant K72357, MNiSW grant N N202 033837, and COPIGAL.

- 
- [1] A. Bohr and B.R. Mottelson, *Nuclear Structure* (Benjamin, New York, 1975), Vol II.
  - [2] O. Haxel, J.H.D. Jensen, and H.E. Suess, *Phys. Rev.* **75**, 1766 (1949).
  - [3] M.G. Mayer, *Phys. Rev.* **75**, 1969 (1949).
  - [4] K. Ikeda, N. Takigawa, and H. Horiuchi, *Prog. Theor. Phys. Suppl. Extra number*, 464 (1968).
  - [5] J. Okołowicz, M. Płoszajczak, and I. Rotter, *Phys. Rep.* **374**, 271 (2003);  
R. Chatterjee, J. Okołowicz, and M. Płoszajczak, *Nucl. Phys. A* **764**, 528 (2006);  
J. Okołowicz, M. Płoszajczak, and Y. Luo, *Acta Phys. Pol.* **39**, 389 (2008);  
Y. Luo, J. Okołowicz, and M. Płoszajczak, *arXiv:nucl-th/0211068*.
  - [6] J. Dobaczewski, N. Michel, W. Nazarewicz, M. Płoszajczak, and J. Rotureau, *Prog. in Part. and Nucl. Phys.* **59**, 432 (2007);  
J. Okołowicz, M. Płoszajczak, and Yan-an Luo, *Acta Phys. Pol.* **39**, 389 (2008).
  - [7] M. Danos and B.M. Spicer, *Z. Physik* **237**, 320 (1970);  
A. Arima, V. Gillet, and J. Ginocchio, *Phys. Rev. Lett.* **25**, 1043 (1970);  
M. Danos and V. Gillet, *Phys. Lett. B* **34**, 24 (1971);  
F. Catara, A. Insolia, and U. Lombardo, *Nucl. Phys. A* **261**, 282 (1976).
  - [8] J.A. Wheeler, *Phys. Rev.* **52**, 1083 (1937);  
C.F. von Weizsäcker, *Naturwiss.* **26**, 209 (1938);  
W. Wefelmeier, *Z. Physik.* **107**, 332 (1937).
  - [9] J. Hiura and I. Shimodaya, *Prog. Theor. Phys.* **30**, 585 (1963); *ibid.* **36**, 977 (1966).
  - [10] R. Tamagaki and H. Tanaka, *Prog. Theor. Phys.* **34**, 191 (1965).
  - [11] D.M. Brink, *In Proceedings of the International School*

- of Physics “Enrico Fermi” Course XXXVI, edited by C. Bloch (Academic, New York, 1966), p. 247.
- [12] Y. Fujiwara, H. Horiuchi, K. Ikeda, M. Kamimura, K. Katō, Y. Suzuki, and E. Uegaki, Prog. Theor. Phys. Suppl. **68**, 60 (1980).
  - [13] S. Drożdż, J. Okołowicz, and M. Płoszajczak, Phys. Lett. B **128**, 5 (1983).
  - [14] W. Bauhoff, E. Caurier, B. Grammaticos, and M. Płoszajczak, Phys. Rev. C **32**, 1915 (1985).
  - [15] T. Neff, and H. Feldmeier, Nucl. Phys. A **738**, 357 (2004).
  - [16] For example, *Proc. of the 8th Int. Conf. on Clustering Aspects of Nuclear Structure and Dynamics*, Edited by K. Ikeda, I. Tanihata, and H. Horiuchi, Nucl. Phys. A **738** (2004).
  - [17] W. von Oertzen, Z. Phys. A **354**, 37 (1996); A **357**, 355 (1997).
  - [18] M. Freer *et al.*, Phys. Rev. Lett. **82**, 1383 (1999).
  - [19] W. von Oertzen, M. Freer, and Y. Kanada-En’yo, Phys. Rep. **432**, 43 (2006).
  - [20] A. Volya and V. Zelevinsky, Phys. Rev. C **74**, 064314 (2006).
  - [21] N. Michel, W. Nazarewicz, M. Płoszajczak, and T. Vertse, J. Phys. G: Nucl. Part. Phys. **36**, 013101 (2009).
  - [22] J. Cseh, J. Darai, A. Algora, H. Yepez-Martinez, and P. O. Hess, Rev. Mex. Fis. S **54** (3), 30 (2008).
  - [23] N. Itagaki, S. Aoyama, S. Okabe, and K. Ikeda, Phys. Rev. C **70**, 054307 (2004).
  - [24] N. Itagaki, A. Kobayakawa, and S. Aoyama, Phys. Rev. C **68**, 054302 (2003).
  - [25] J.J. Griffin and J.A. Wheeler, Phys. Rev. **108**, 311 (1957).
  - [26] N. Itagaki, H. Masui, M. Ito, and S. Aoyama, Phys. Rev. C **71** 064307 (2005).
  - [27] H. Masui, N. Itagaki, Phys. Rev. C **75** 054309 (2007).
  - [28] P. Cejnar and F. Iachello, J. Phys. A **40**, 581 (2007); J. Cseh, J. Darai, H. Yepez-Martinez, and P. O. Hess, Int. J. Mod. Phys. E **17**, 2296 (2008); P. Cejnar and J. Jolie, Progr. Part. Nucl. Phys. **62**, 210 (2009); F. Iachello, AIP Conf. Proc. **1165**, 193 (2009).
  - [29] J. Cseh, J. Phys. Conf. Ser. **205**, 012021 (2010).
  - [30] These components are necessary because the spin-orbit interaction has the form of  $\vec{l} \cdot \vec{s}$ , and both spatial part ( $\vec{l}$ ) and spin part ( $\vec{s}$ ) are time odd.
  - [31] A. Ono, H. Horiuchi, T. Maruyama, and A. Ohnishi, Prog. Theor. Phys. **87**, 1185 (1992); Phys. Rev. Lett. **68**, 2898 (1992).
  - [32] H. Feldmeier, Nucl. Phys. A **515**, 147 (1990).
  - [33] S. Drożdż, J. Okołowicz, and M. Płoszajczak, Phys. Lett. B **109**, 145 (1982); E. Caurier, B. Grammaticos, and T. Sami, Phys. Lett. B **109**, 150 (1982).
  - [34] The cluster width  $\nu$  becomes a complex parameter and is allowed to vary in the TDC [33] and FMD [32] approaches.
  - [35] H. Feldmeier, K. Bieler, and J. Schnack, Nucl. Phys. A **586**, 492 (1995).
  - [36] J. Da Providência, Nucl. Phys. **46**, 401 (1963); D.K. Kerman, and S.E. Koonin, Ann. Phys. **100**, 332 (1976).
  - [37] A.B. Volkov, Nucl. Phys. **74**, 33 (1965).
  - [38] R. Tamagaki, Prog. Theor. Phys. **39**, 91 (1968).
  - [39] S. Okabe and Y. Abe, Prog. Theor. Phys. **61**, 1049 (1979).
  - [40] T. Matsuse, M. Kamimura, and Y. Fukushima, Prog. Theor. Phys. **53**, 706 (1975); Y. Fukushima, M. Kamimura, and T. Matsuse, Prog. Theor. Phys. **55**, 1310 (1976).
  - [41] K. Katō and H. Bandō, Prog. Theor. Phys. **59**, 774 (1978).
  - [42] Y. Fujiwara, H. Horiuchi, and R. Tamagaki, Prog. Theor. Phys. **61**, 1629 (1979); Y. Fujiwara, Prog. Theor. Phys. **62**, 122 (1979).
  - [43] Y. Akiyama, A. Arima, and T. Sebe, Nucl. Phys. A **138**, 273 (1969).
  - [44] J.B. McGrory and B.H. Wildenthal, Phys. Rev. C **7**, 974 (1978).
  - [45] T. Tomoda, A. Arima, Nucl. Phys. A **303**, 217 (1978).
  - [46] S. Hara, K. T. Hecht, and Y. Suzuki, Prog. Theor. Phys. **84**, 254 (1990); S. Hara, K. Ogawa, and Y. Suzuki, Prog. Theor. Phys. **84**, 254 (1992).
  - [47] Y. Kanada-En’yo and H. Horiuchi, Prog. Theor. Phys. **93**, 115 (1995).
  - [48] Y. Taniguchi, M. Kimura, and H. Horiuchi, Prog. Theor. Phys. **112**, 475 (2004).
  - [49] T. Yamada, Phys. Rev. C **42**, 1432 (1990).
  - [50] T. Terasawa, Prog. Theor. Phys. **23**, 87 (1960); A. Arima and T. Terasawa, Prog. Theor. Phys. **23**, 115 (1960).
  - [51] T. Myo, K. Katō, and K. Ikeda, Prog. Theor. Phys. **113**, 763 (2005).
  - [52] T. Otsuka, T. Suzuki, R. Fujimoto, H. Grawe, and Y. Akaishi, Phys. Rev. Lett. **95**, 232502 (2005).
  - [53] D.J. Rowe, Nucl. Phys. A **745**, 47 (2004).
  - [54] F. Iachello, Phys. Rev. C **23**, 2778 (1981); F. Iachello and R.D. Levine, J. Chem. Phys. **77**, 3046 (1982).
  - [55] J. Cseh, Phys. Lett. B **281**, 173 (1991); J. Cseh and G. Lévai, Ann. Phys. (NY) **230**, 165 (1994).
  - [56] J. Cseh, J. Phys. Soc. Jpn. **58** Suppl. 604 (1989).
  - [57] H. Yepez-Martinez, J. Cseh, and P. O. Hess, Phys. Rev. C **74**, 024319 (2006).
  - [58] J.P. Elliott, Proc. Roy. Soc. **245**, 128 (1958).
  - [59] D.J. Rowe, C. Bahri, and W. Wijesundera, Phys. Rev. Lett. **80**, 4394 (1998).
  - [60] A. Frank, J. Jolie, P. Van Isacker, Symmetries in Atomic Nuclei, Springer, New York (2009).
  - [61] C. Vargas, J.G. Hirsch, P.O. Hess, J.P. Draayer, Phys. Rev. C **58**, 1488 (1998); C. Vargas, J.G. Hirsch, J.P. Draayer, Nucl. Phys. A **690**, 409 (2001).
  - [62] D.J. Rowe, Rep. Prog. Phys. **48**, 1419 (1985), and references therein.
  - [63] G. Rosensteel and D.J. Rowe, Phys. Rev. Lett. **47**, 223 (1981).
  - [64] O. Castanos, J.P. Draayer, Nucl. Phys. A **491**, 349 (1989).